Sixth International Symposium on Marine Propulsors
smp'19, Rome, Italy, May 2019

Coupled Numerical Simulation and Modal analysis of Composite Ducted Propeller

Xiaoyi An[1,2], Baowei Song[1], Hui Xia[1], Yongle Ding[1], Zhihui Jin[1], Larry Lessard[2]

[1] School of Marine Science and Technology, Northwestern Polytechnical University, Xi'an, China
[2]Department of Mechanical Engineering, McGill University, Montreal, Canada

ABSTRACT

With the rapid development of composite materials throughout the world, the use of advanced materials has become very common on marine propellers. Compared to metals, composite materials have many advantages such as light weight, high strength-to-weight ratio and reduced noise properties. The anisotropic nature of carbon fiber reinforced plastic (CFRP) with different stacking sequences and fiber angles can be used to build a composite propeller with enhanced hydrodynamic and mechanical properties. The primary objectives of this paper are to analyze the fluid-structure interaction (FSI) and modal properties of the composite ducted propeller. The solid model of the propeller is developed with Unigraphics NX 9.0. The composite structures are established with ANASYS-ACP. FSI analysis of both metallic and composite propellers are carried out on CFD (Computational Fluid Dynamic) coupled with FEM (finite element method). Several finite element models with different stacking sequences and ply orientations of the propeller are analyzed. An acceptable layup for the composite blade is found. The hydrodynamic performance and mechanical properties of both composite and metallic ducted propellers are discussed.

Keywords

Fluid-structure interaction, Composite, ducted propeller, Modal analysis.

1 INTRODUCTION

In the past, most of the maritime industry used manganese-nickel-aluminum-bronze (MAB) or nickel-aluminum-bronze (NAB) as the primary material for propeller construction. This was done for many reasons such as its superior corrosion resistance high-yield strength, reliability, and affordability (Young, 2008). However, it is heavy, expensive, and creates noise and vibration in complex propeller geometries. As an alternative, composite propellers take advantage of the outstanding material properties of composites such as light weight, high strength-to-weight ratio, high stiffness-to-weight ratio and greater geometrical design flexibility. Light composite materials can make the blades thinner and more flexible to improve the hydrodynamic performance. Moreover, composites can bring us the potential benefits of reduced corrosion and cavitation damage, improved fatigue performance, reduced noise, improved material damping properties, reduced manufacturing cost and life time maintenance cost (Motley et al. 2009).

Flexible composite marine propellers have several advantages over conventional rigid metallic propellers. In particular, composite propellers have great potential for performance improvement. The use of composites on the blades can lead to reduced fuel consumption, engine workload, absorbed horsepower and operating life, the engine and shaft vibration by around 25% and lead to less noise and hull vibration (Ashkenazi dt al., 1974). Fluid-structure interaction effects are used to improve the performance of composite marine propellers under a wide range of operating conditions (Young et al. 2016).

Compared with the conventional propulsion propeller, the ducted propellers are very useful propulsion units by providing advanced operability and higher bollard thrust to support marine vessels (Funeno, 2017). It is used to improve the efficiency of the propeller and is especially used on heavily loaded propellers or propellers with limited diameter. A lot of experimental and theoretical researchers have been done on ducted propeller (Hoekstra,2006; Oosterveld, 1970).

In this paper, the hydrodynamic performance analysis of the mental ducted propeller model with fluid-structure interaction method is firs performed. Comparing the simulation results with the experiment data, determines the validity of FSI analysis process. Then, several structure finite element models of the composite ducted propeller with different layups of carbon fiber reinforced plastic

[*] Leave blank the last 2.0 cm on the first page to place some additional informational about this paper in a footnote on the first page if necessary.

(CFRP) are built and examined. Analysis is done to check the mechanical performance and modal properties of the propeller with different stacking sequences and ply angles, so that the most suitable layup for the ducted propeller is found. Finally, the fluid-structure coupling simulation of the composite ducted propeller with the best structure from finite element modeling is presented. The hydrodynamic performance, mechanical properties and modal properties of the composite ducted propeller are compared to the metallic propeller.

2 NUMEICAL METHOD

In this paper, the numerical simulations are carried on a standard ducted propeller, model of Ka4-70 with 19A duct, which was presented by MARIN (Maritime Research Institute Netherland) (Oosterveld, 1970). As shown in Figure 1, the ducted propeller consists of composite blades with metal hub and duct. The diameter of the ducted propeller is D=240mm. The pitch-diameter ratio is P/D=1. The tip clearance of the duct is 1 mm, which is the standard distance in the experimental results.

Figure1: composite ducted propeller model

2.1 Fluid Domain and Boundary Conditions

In this analysis, we divide the solution field into two parts—the stationary domain and the rotating domain as shown in Figure 2. The Stationary domain should be large enough to insure the outer boundary will not influence the analysis of the near-propeller fluid flow. To improve the calculating efficiency, periodic boundary conditions using 1/4 of the rotating domain is applied. The 1/4 model gives the same result as the model of the whole rotating part. The stationary domain is meshed with structured elements while the rotating domain is meshed with unstructured elements. Previous work shows that the combination of both types of mesh can improve the calculation efficiency (Morgut at al. 2012).

The numerical analysis presented in this paper is carried out by a CFX solver to evaluate the hydrodynamic performance of the ducted propeller and transmit the data between the solid and fluid regions. The governing equation of the problem is solved by the RANS equation. The fluid is assumed as an incompressible fluid. The SST model is used for a turbulence model and the turbulence intensity of the velocity inlet boundary is imposed to 1%. On the outlet boundary, the static pressure outlet with 0 Pa

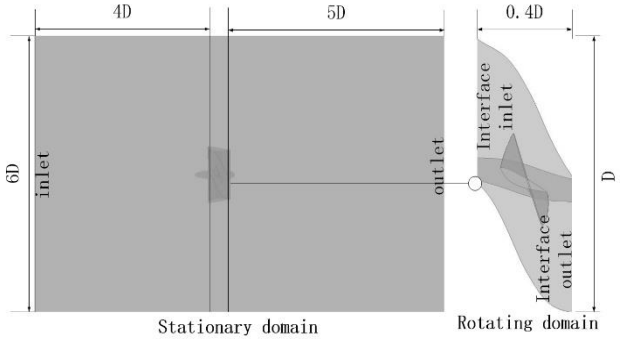

Figure 2: Calculation domain

reference pressure is imposed. The rotating speed of the inside domain is set to 7.5 RPS. The propeller blades are modeled as an ANSYS Multifield wall by which one could achieve the data transmission between the blades and fluid. The duct and the hub are imposed to no slip along the wall.

Table 1: Material properties

Material Property	Copper Alloy	CFRP
Young's Modulus (GPa)	E=110	E1=123 E2=7.78 E3=7.78
Shear modulus (GPa)	G=41	G_{xy}=5.00 G_{yz}=3.08 G_{xz}=5.00
Poisson ratio	V=0.34	V_{xy}=0.27 V_{yz}=0.42 V_{xz}=0.27
Density (ton/m^3)	ρ=8.3	ρ=1.6

2.2 Solid Model and Boundary Conditions

ANSYS transient structural analysis is used for structural setups. The total time is set to 4s, and the timestep is set to 0.02s. This is the same setting in the CFX solver to make sure that success of the FSI analysis is achieved. The fluid solid interface is applied to the propeller blades. A fixed support is defined at the root of the blade.

Table 2: Stacking sequence and reference direction

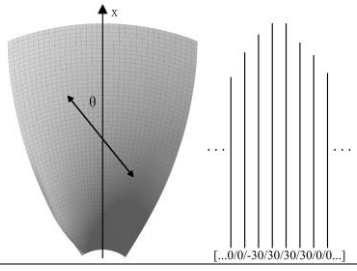	$[0_2/\pm30]_s$
	$[0_4/\pm30]_s$
	$[0_4/\pm45]_s$
	$[0_4/\pm60]_s$
	$[0_4/\pm90]_s$

In this present paper, we use two materials for the propeller blades: copper alloy and unidirectional carbon fiber reinforced polymer. Both properties are shown in Table 1.

For the composite propeller, the characteristics are calculated for five different stacking sequences. The five different layups of the ducted propeller FEM model are shown in Table 2. The generation line (x-axis) shown to the left of the table is set as the reference line of fiber orientation of the composite material. The angle θ, measured from the reference line, represents the zero-degree direction.

3. METAL PROPELLER PERFORMANCES

To evaluate the hydrodynamic performance of marine propellers, the following non-dimensional coefficients are given: the advance ratio J, total thrust coefficient K_T, duct thrust coefficient K_{TN}, torque coefficient K_Q, and efficiency η. Which can be calculated through equations (1) and (2) as follows:

$$K_T = \frac{T}{\rho n^2 D^4}, K_{TN} = \frac{T_N}{\rho n^2 D^4}, K_Q = \frac{Q}{\rho n^2 D^5} \quad (1)$$

$$\mathrm{J} = \frac{V_A}{nD}, \eta = \frac{J}{2\pi}\frac{K_T}{K_Q} \quad (2)$$

Where V_A = advance speed; n = rotation speed (RPS); D = propeller diameter; ρ = density of water and Q = blade torque. The total thrust of the ducted propeller is $T = T_P + T_N$, where T_P and T_N, respectively, represent the blade thrust and duct thrust.

3.1 Validation

After solving the fluid-structure interaction of the ducted propeller with copper alloy material, the computational results of thrust, torque and efficiency, compared with experimental data, are shown in Figure 3. It shows that the computed results of the ducted propeller's open-water characteristics are in good agreement with the experimental results.

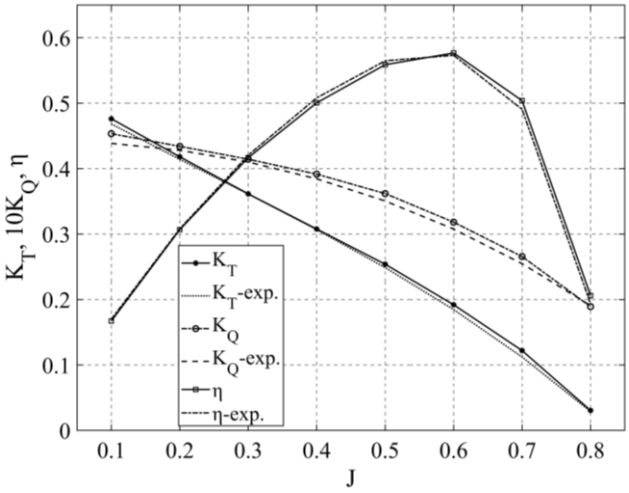

Figure 3: Comparison between the numerical and experimental results for metal ducted propeller

The calculation results under non-FSI method and FSI method for the ducted propeller compared with the experimental results are listed in Table 3. It shows that the results analyzed through fluid-solid interaction method have a better agreement compared to the results that did not use the coupling method.

Table 3: Calculation error (J=0.6)

	Error of K_t (%)	Error of K_q (%)	Error of η (%)
Non-FSI	4.001	3.417	0.612
FSI	2.912	2.953	0.007

3.2 results and discussion

Figure 4 presents the pressure distribution of the metal ducted propeller on both sides of the blade and the inner face on the duct. It is clear from the figure that on the face side, the pressure decreases gradually from the leading edge to the middle of the face and then increases to the trailing edge. On the back side of the blade, the pressure increases gradually from the leading edge to the trailing edge. The mutual effect of the propeller between the duct and the top of the blade caused distinct pressure drops at the leading edge and at the blade tip. It can be seen on the inner face of the duct that there is a low-pressure area at the tip clearance extending from the tip of the propeller blade due to the acceleration of the fluid.

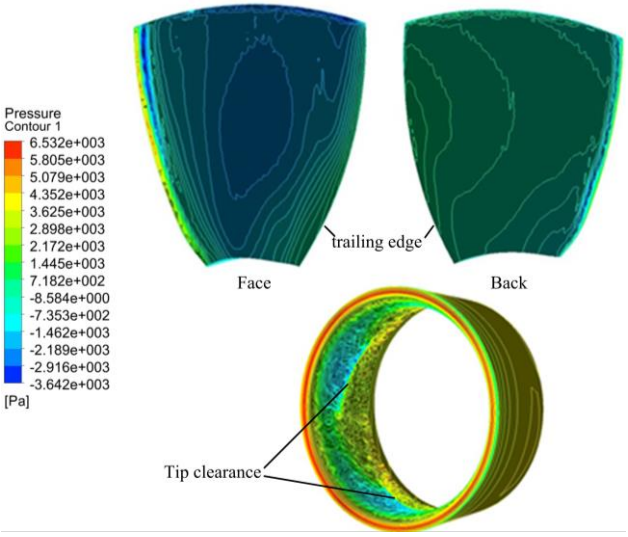

Figure 4: Pressure distribution of ducted propeller at J=0.6

The equivalent Von-Mises stress distribution in the face and back of the ducted propeller blade is shown in Figure 5. The stresses are concentrated close to the middle of the blade root area and as we move to the other sections of the blade, the stresses decrease gradually. The stress field decreases with the growing values of the radius and drop to small values in the region near the tip and trailing edge of the blade. This distribution of stress makes practical

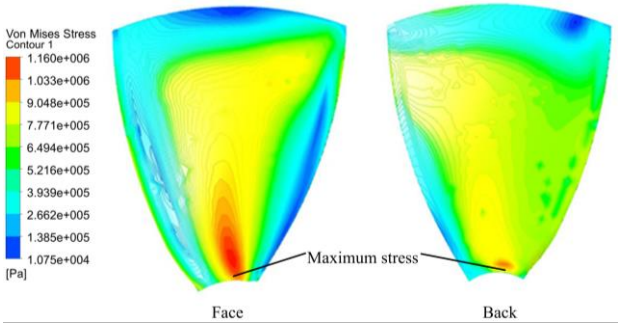

Figure 5: Stress distribution of the propeller blade at J=0.6

sense, because blades are fixed on the propeller hub at the root and bent by the hydrodynamic pressure on the surfaces.

To investigate the influence of the tip clearance on the ducted propeller, several gap values (from 0.5mm to 3.0mm) between the tip of blade and the inner face of duct were set by changing the diameter of the duct. This ducted propeller reaches maximum efficiency at about $J = 0.6$. Therefore, we choose $J = 0.6$ as the main analysis condition.

The flow leaking through the tip clearance causes a change in the hydrodynamic properties of the propeller. The variation of duct thrust coefficient, total thrust coefficient, torque coefficient and efficiency under different gap sizes of the propeller are given in Figure 6. In general, the duct thrust coefficient and efficiency decrease while the gap expands. The slope of the two lines are near -2.919×10^{-3} and -4.488×10^{-3}, respectively. As shown, the total thrust coefficient and torque coefficient of the propeller increases along the gap expending axis. The slops of these two lines both change suddenly when the gap expends to 2 millimeters.

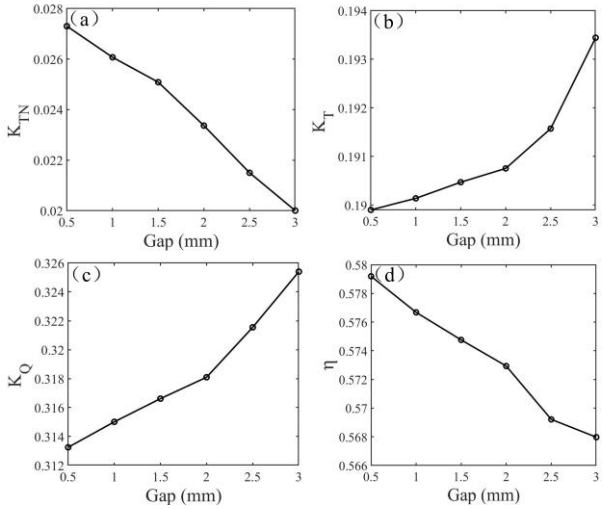

Figure 6: Variation of (a)duct thrust coefficient

(b)total thrust coefficient (c)torque coefficient and (d) efficiency

4. COMPOSITE PROPELLER PERFORMANCES

To analyze the influence of different ply angle and stacking sequences on the ducted propeller blades, five different FEM models of the ducted propeller were analyzed with hydrodynamic pressure. The results and discussions are as follows.

4.1 Comparison among five FEM models

4.11 deformation property

Figure 7 demonstrates the deformation distribution and direction on the ducted propeller with $[0_4/\pm30]$s layup on tip of the blade under working condition J=0.6. It is clear that the deformation mainly appears on the top part of the blade and it undergoes both bending and twisting. The maximum deformation is located on the t op of the trailing edge. We use non-dimensional coefficient L=a/C to determine the location on the tip of the blade. Where a is the length measured from the leading edge; C is the length of the entire edge.

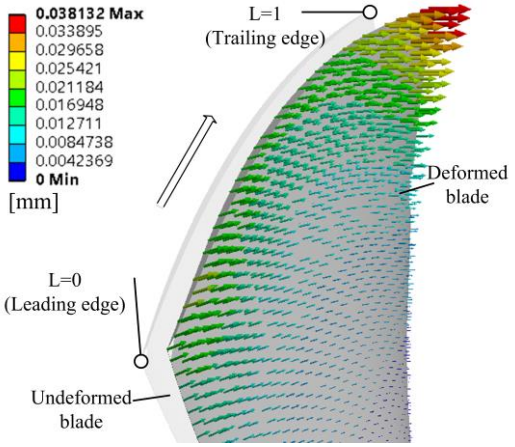

Figure 7: Deformation on tip of the blade ($[0_4/\pm30]$s layups)

The variation of deformation value at the tip of the blade with different layups, is shown in Figure 8. We can see that the blade undergoes less deformation under the hydrodynamic pressure at around 0.5L, and it goes to the minimum value when using the $[0_4/\pm30]$s stacking sequence. All five curves reach the maximum value at 1L, and the blade undergoes more deformation with $[0_4/\pm90]$s layup. In comparing the propeller made of $[0_2/\pm30]$s layup with the one made of $[0_4/\pm30]$s layup, more layers of composites with 0-degree ply angle provide more flexure strength at the middle of the blade, where the blade mainly undergoes the bending deflection. The twisting deflection on the blade has a strong effect near the trailing edge at around 0.8L to 0.9L, where the slope of the curves increases rapidly. When layups with the same amount of 0-degree ply layers are applied on the blades, 30-degree and 45-degree ply angles show better bending resistance ability.

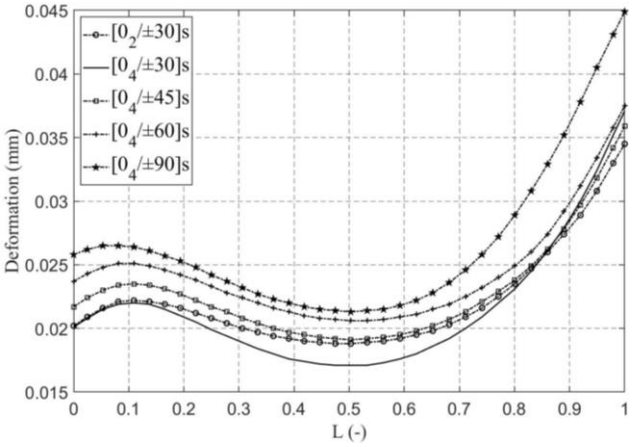

Figure 8: Variation of deformation on tip of the blade

4.1.2 failure criterion

To analyze the structural behavior of the composite ducted propeller blade in this paper, the five FEM models of composite propeller are evaluated by the Tsai-Wu failure criterion, which is widely used for anisotropic materials (that have different strengths in tension and compression) (Tsai at al 1971). In the criterion, the material is broken if the failure index is equal to or greater than 1, while the

composite has enough strength when the value is less than 1.

Figure 9 demonstrates the distribution of the Tsai-Wu failure index on a typical blade. The failure index increases when the thickness changes via reducing the number of layers in the element. The most critical region is at the tip of the blade at around 0.9L, where it shows that the maximum failure index values are between 0.009 and 0.011 which means the present composite layup is well within the factor of safety.

After analyzing the failure characters of all five composite ducted propellers, the failure indices along the tip edge of the blades are demonstrated in Figure 10. Compared with the deformation distribution at the tip of blade in Figure 8, the highest maximum failure index values occur at around 0.8L to 0.9L at the tip, where the blade undergoes the strongest twisting deflection. Comparing the propeller made of $[0_2/\pm30]$s layup with the one made of $[0_4/\pm30]$s layup, composites with 30-degree plies provide more flexure strength at the location around 0.9L of the blade, where the deflection direction is more perpendicular to the 30-degree fiber direction.

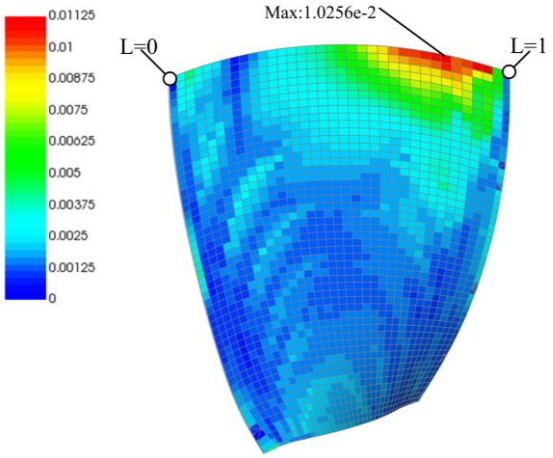

Figure 9: Tsai-Wu failure index distribution ($[0_4/\pm30]$s layups)

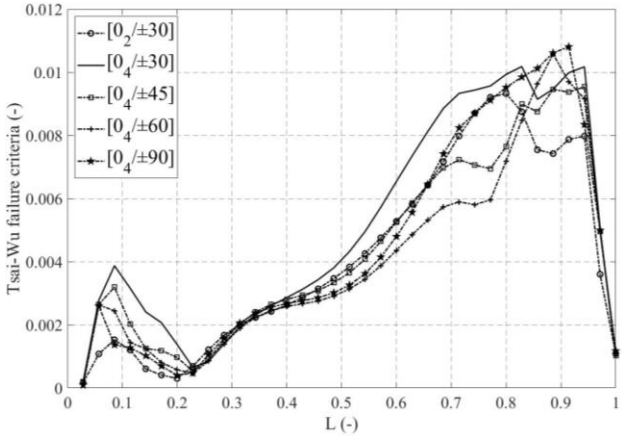

Figure 10: Variation of Tsai-Wu failure index on tip of the blade

4.1.3 Modal analysis

As the mode shapes of the five ply stacking sequences models are almost the same, we present the first three modes of vibration of the ducted propeller blade with $[0_4/\pm30]$s stacking sequence, in Figure 11. The first mode

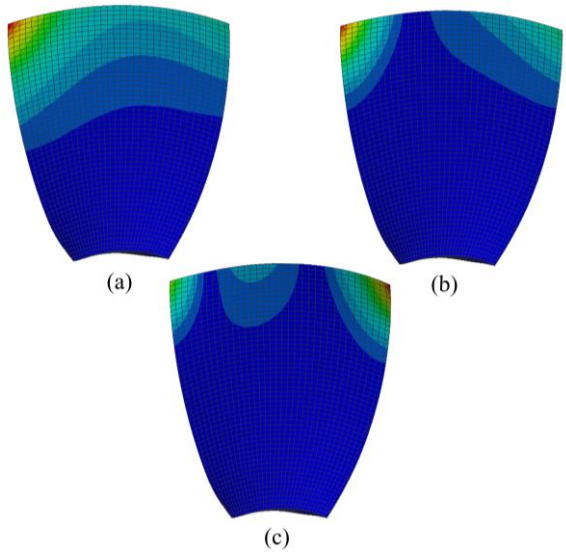

Figure 11: Vibration modes of blade with $[0_4/\pm30]$s stacking sequence. (a) mode I; (b) mode II and (c) mode III

is pure bending mode and the second mode is pure torsion mode. The third mode is a secondary bending and torsion mode in the direction of the span.

Table 4 presents the first three natural frequencies of the ducted propeller blade from five different stacking sequences models. Compared with the blade made of $[0_2/\pm30]$s layup, the blade with $[0_4/\pm30]$s layup has higher natural frequencies, which means more 0-degree plies can improve the natural frequency of the blade. The natural frequencies of the blade with $[0_4/\pm30]$s layup exceed those of the other blades that have the same number of 0-degree plies. Therefore, more 0-degree plies with 30-degree plies layups can improve the natural frequencies of the ducted propeller.

Table 4: Natural frequency (Hz) of composite propeller blade

Mode	1	2	3
$[0_2/\pm30]_s$	1203.9	1769.5	2298.5
$[0_4/\pm30]_s$	1210.8	1694.2	2211.9
$[0_4/\pm45]_s$	1182.3	1765.7	2323.6
$[0_4/\pm60]_s$	1147.7	1810.0	2330.9
$[0_4/\pm90]_s$	1110.6	1674.7	2080.4

4.2 Hydrodynamic performance of composite propeller

As we analyzed above, the $[0_4/\pm30]$s stacking sequence shows better mechanical properties for the ducted propeller blade than other stacking sequences. The hydrodynamic coefficients, composed of total thrust coefficient, torque coefficient and efficiency are compared between the metal model and a composite model with $[0_4/\pm30]$s layups in the same ducted propeller geometry are shown Figure 12. In general, the composite propeller gives lower efficiency relative to the metal propeller, especially at high advance ratio. Combining with the deformation and pressure analysis, we can see that due to the higher pressure on the face side, the blade tends to bend toward the upstream direction. Consequently, the hydrodynamic performance

decreases. The efficiency decreases because the reduction in thrust is higher than the reduction in torque.

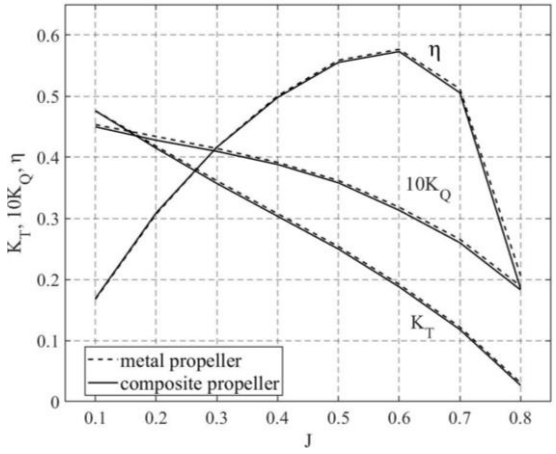

Figure 12: Hydrodynamic coefficients of metal and composite ducted propeller

Figure 13 shows the maximum deformation of the composite ducted propeller with $[0_4/\pm30]$s versus the advanced velocity ratio. We can see that with the increases of advance velocity ratio, the maximum deformation value of the blade decreases. Therefore, the maximum deflection for the composite propeller occurs at J = 0.1. The maximum deformation on the metal propeller is close to 0mm, which could be interpreted as a rigid body.

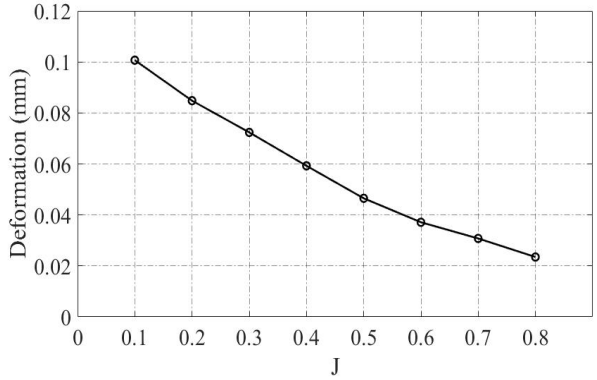

Figure 13: Deformation of the blade versus advance ratio

The changes of pressure distribution over time in the static domain is illustrated in Figure 14. It is obvious that the pressure distribution from 0s to 1s undergoes an unsteady process and trend is to be steady after about 1s. The Changes of the efficiency of the ducted propeller over time at J = 0.6 are demonstrated in Figure 15. The efficiency decreases gradually from 0s and trend fluctuates around 0.5734 after 1s, which indicates the fluid-structure interaction between the blade and water.

Figure 16 shows the pressure distribution contours on the five cross sections in the rotating domain at J = 0.6, which are perpendicular to the propeller shaft (from x = 0.02m to x = -0.02m along the downstream direction). It is obvious that the fluid is accelerated toward the downstream direction under the impact of the propeller operation. The balance of pressure distribution in the rotating domain decreases towards the downstream direction. The tip clearance between the blade and the inner face of the duct has a strong influence on the pressure distribution. This explains the pressure drop on the tip of the blades and the inner face of the duct close to the blades.

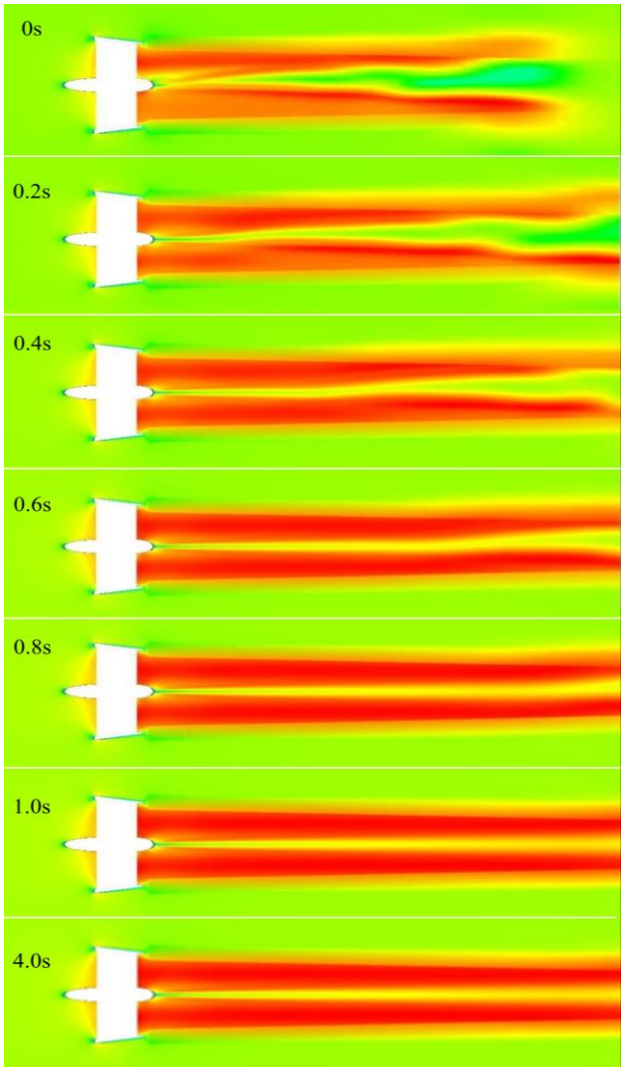

Figure 14: Change of pressure at static domain

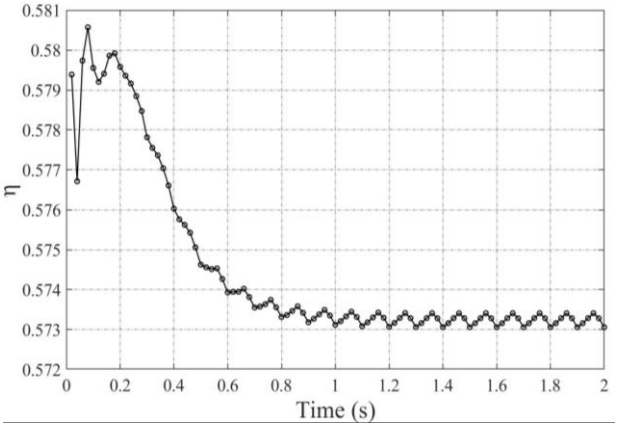

Figure 15: Change of efficiency over time domain at J = 0.6

The modal shapes of the composite propeller blades are similar to the metal ones. The first three natural frequencies of both composite and metallic blades are shown in Table 5. While the composite blades show higher natural frequencies than the metal ones. The first modal frequency on the composite blade is almost twice that of the metallic blade.

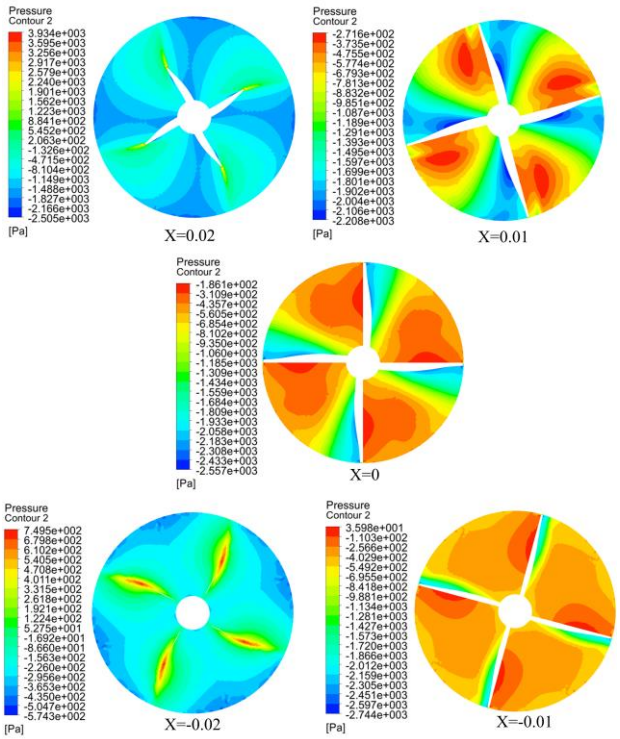

Figure 16: pressure distribution on cross section

5. Conclusion

In the present paper, a coupled numerical simulation is used to investigate the hydrodynamic and mechanical behavior of a composite ducted propeller. The FSI method is validated by comparing the calculation results with the experimental results. The main results discussed in this paper are as follows:

a) The pressure and Von-Mises stress distribution are presented and the influence of the tip clearance on the metallic ducted propeller is investigated. It shows that the total thrust and torque coefficient increases linearly with the gap expanding at designed working conditions, whereas the efficiency decreases.

b) Five FEM models with different stacking sequences are analyzed. Results show that the composite blade deformed under both bending and twisting effect. More 0-degree plies provide better support at the middle of the blade, where it mainly undergoes bending deflection. 30-degree and 45-degree plies show better bending resistance ability in the twisting region. The highest maximum failure index values occur at around 0.8L to 0.9L on the tip of blade, where the blade undergoes the strongest twisting deflection. The first, second and third modes are the first bending, torsion and second bending and torsion modes in the direction of the span, respectively. Using a Combination of more 0-degree plies with 30-degree layups can improve the natural frequencies of the ducted propeller.

c) A comparison between composite and metallic ducted propeller for open-water performance and mechanical properties are analyzed. The results show that the efficiency of composite ducted propeller decreases because the reduction in thrust is higher than the reduction in torque. The composite blades show higher natural frequencies than the metal ones. The natural frequency of the metallic blade is almost 50% lower than the composite blade.

Table 5: Natural frequency (Hz) of propeller blade

Mode	Metal blade	Composite blade
1	622.04	1210.8
2	1310.9	1694.2
3	1497.8	2211.9

In this research, the FSI and modal analysis of composite propeller are presented. Results show the modal properties of composite are better than the metallic propeller, while hydrodynamic performance of the composite ducted propeller decreases slightly. Hence further work should be carried on the design and optimization of stacking sequences and ply angles based on the results analyzed in this paper, to obtain a proper model of a self-adaptive propeller.

REFERENCES

Young, Y. L. (2008). 'Fluid-Structure interaction analysis of flexible composite marine propellers', Journal of Fluid and Structures. 24(6): p. 799-818

Young, Y. L., Motley, M. R., Barber, R., Chae, E. J., Garg, N., (2016). 'Adaptive Composite Marine Propulsors and Turbines: Progress and Challenges'. Applied Mechanics Reviews. Vol. 68.

Motley, M. R., Z. Liu, and Young, Y. L. (2009), 'Utilizing fluid-structure interactions to improve energy efficiency of composite marine propellers in spatially varying wake.' Composite Structures. 90(3): p. 304-313.

Ashkenazi, Y., Gol'fman, I., Rezhkov, L., Sidorov N. (1974), Glass-Fiber-Reinforced Plastic Parts in Ship Machinery. Sudostroyenniye Publishing Houe, Leningard.

Funno, I. (2017), 'Influence of hydrodynamic interaction between ducted propellers and struts on performance of azimuth thrusters', Fifth International Symposium on Marine Propulsors, Finland.

Hoekstra, M. (2006). 'A RANS-based analysis tool for ducted propeller systems in open water condition', International shipbuilding progress, 53(3), pp.205-227.

Oosterveld, M. W. C., (1970. 'Wake adapted ducted propellers', Delft University of Technology.

Morgut, M., Nobile E., （2012）. 'Influence of grid type and turbulence model on the numerical prediction of the flow around marine propellers working in uniform inflow'. Ocean Engineering. 42, pp.26-34.

Tsai, S.W., Wu, E. M. (1971). 'general theory of strength for anisotropic materials', Journal of Composite Materials. Vol. 5, pp. 58-80.

Lin, H. J., Lai, W. M., Kuo, Y. M. (2010), 'Effects of stacking sequence on nonlinear hydroelastic behavior of composite propeller blade'. Journal of Mechanics. vol. 26, pp.293-298.

Gopaiah, D., Nageswararao, N. A. (2014), 'Design and analysis of composite propeller using ANSYS'. IOSR Journal of engineering. Vol. 04, pp.48-59.